Experimental Report

16/02/2010

Proposal: **5-24-384** **Council:** 10/2008

Title: Phase behaviour and thermoelastic properties of ammonia monohydrate (ND3•D2O) phases I and II.

This proposal is a new proposal

Researh Area: Soft condensed matter

Main proposer: **FORTES Andrew Dominic**

Experimental Team: FORTES Andrew Dominic

Local Contact: SUARD Emmanuelle
LEMEE-CAILLEAU Marie-Helene

Samples: Ammonia monohydrate, ND3.D2O

Instrument	Req. Days	All. Days	From	To
D2B	2	2	18/05/2009	20/05/2009

Abstract:

Ammonia-water solid mixtures are of great importance in modelling of solar system ices. Ammonia monohydrate exists in a number of polymorphs; however, the physical properties of these polymorphs have not yet been measured, and the structures of the higher-pressure phases are unknown. I propose to measure the incompressibility of the ambient-pressure phase (AMH I), observe the phase transition to phase II and collect data for determination of the thermophysical properties of AMH II. The powder specimen will be melted in situ, and regrown as one (or very few) large single crystals in the gas cell, and then transferred to the single crystal diffractometer, Vivaldi. From previous powder measurements it has been possible to index AMH II but no satisfactory structure solution has been obtained. Analysis on Vivaldi will allow the structure to be found.

Introduction

Ammonia hydrates are likely to be important 'rock'-forming minerals in the outer solar system, and determination of their behaviour at high-pressure is necessary for accurate modeling of the interiors of icy satellites. Ammonia hydrates are also likely to be 'rock'-forming minerals on the solid bodies of the outer solar system, giant icy moons such as Ganymede, Callisto and Titan. The high-pressure behavior must be known in order to model the internal structure and geodynamics of these planetary bodies. The ammonia hydrates are the simplest solids to contain the mixture of homo-nuclear O—H···O and hetero-nuclear O—H···N and N—H···O hydrogen bonds typically found in biomolecules, including DNA. Experimental and computational study of these systems as a function of the thermodynamic variables, P and T, therefore provides an insight into the parameters involved in interatomic potential functions in hydrogen bonded molecular crystals. In earlier work (Fortes *et al.*, 2009a), it was found that a high-pressure polymorph of ammonia dihydrate, ADH II, dissociates upon warming at 550 MPa to a mixture the $R\bar{3}$ phase ice II, and a phase identified only as AMH II. Whilst the latter was indexed with an orthorhombic unit-cell, attempts to solve the structure using the mixed-phase powder data were not successful, and the correct space-group was not determined unambiguously.

Experimental method

The experiment was carried out on a sample of nominal composition $ND_3 \cdot D_2O$ (AMH) prepared by condensing ND_3 gas (Aldrich Chemicals Co., 99 atom % D) into an evacuated glass bulb which was cooled to 215 K in a bath of acetone cooled by dry ice. The bulb was then weighed and the contents diluted to the appropriate stoichiometry with D_2O (Aldrich Chemicals Co., 99 atom % D). Neutron powder diffraction data were collected using a $Ti_{66}Zr_{34}$ null-scattering-alloy gas cell (ILL code 03PG50TZ7: sample Ø7 mm by 30 mm high), connected to a helium gas intensifier. The empty pressure vessel was suspended in a bath of liquid nitrogen the specimen was introduced into the pressure cell using a cooled glass pipette, where it froze immediately: the cell was then quickly screwed onto the cryostat centre stick, pressurized to 100 bar (10 MPa) and mounted in the cryostat.

AMH I was crystallized in the pressure vessel data were collected in the standard 'high-flux' mode of D2B (Ge [335] monochromated radiation, λ = 1.59432 Å, 200 mm horizontal slits) at 180 K, in 25 MPa increments from 102.1—351.0 MPa and 50 MPa increments from 351.0—502.2 MPa. At a pressure of 351 MPa the diffraction pattern was observed to change over the course of 90 minutes from that of the low-pressure phase AMH I, to the diffraction pattern observed previously from the high-pressure phase AMH II. Once the transformation was completed, a second 90 minute measurement at 351 MPa was done to ensure a phase-pure AMH II dataset at this pressure. The P/T points at which the measurements were made is shown in **Figure 1**, which illustrates the low-pressure phase diagram of AMH for context.

At 500 MPa, the highest pressure achievable with the ILL TiZr cell, two long integrations were made in order to provide data suitable for testing structural models of AMH II, one using the 'high-resolution' mode of D2B (λ = 1.59432 Å, horizontal slits reduced to 100 mm), the other using one of the longer wavelength options (Ge [331] monochromated radiation, graphite filtered, λ = 2.39845 Å, 200 mm horizontal slits).

Figure 1

Pressure-temperature phase diagram of ammonia monohydrate. The solid vertical line indicates where we believe the equilibrium AMH I → II phase boundary to be, and the dashed line indicates the likely effect of sluggish low-temperature kinetics on the observed position of the AMH I → II phase boundary.

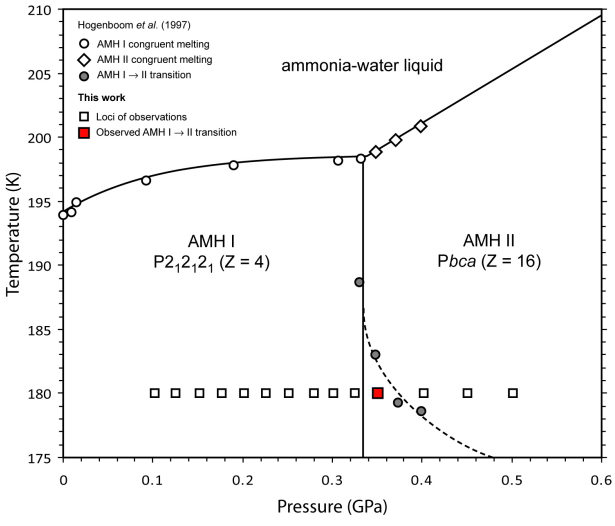

Results

Table 1: Refined unit-cell parameters, unit-cell volume, and axial ratios as a function of pressure from perdeuterated AMH I.

Pressure (MPa)	*a*-axis (Å)	*b*-axis (Å)	*c*-axis (Å)	*b/a*	*c/a*	Unit-cell volume (Å^3)
102.1	4.5083(3)	5.5924(5)	9.7050(6)	1.2405(1)	2.1527(2)	244.68(2)
125.9	4.5035(3)	5.5865(5)	9.6962(7)	1.2405(1)	2.1530(2)	243.95(2)
152.1	4.4983(3)	5.5813(6)	9.6859(8)	1.2408(2)	2.1532(2)	243.18(3)
177.2	4.4935(3)	5.5754(6)	9.6763(8)	1.2408(2)	2.1534(2)	242.42(3)
201.8	4.4887(3)	5.5698(6)	9.6678(8)	1.2408(2)	2.1538(2)	241.71(3)
226.3	4.4844(3)	5.5635(6)	9.6588(8)	1.2406(2)	2.1539(2)	240.97(3)
251.7	4.4803(3)	5.5578(6)	9.6510(8)	1.2405(2)	2.1541(2)	240.31(3)
279.8	4.4747(3)	5.5514(6)	9.6411(8)	1.2406(2)	2.1546(2)	239.49(3)
301.9	4.4713(3)	5.5466(6)	9.6344(8)	1.2405(2)	2.1547(2)	238.94(3)
325.6	4.4668(3)	5.5414(6)	9.6263(8)	1.2406(2)	2.1551(2)	238.28(3)
351.0	4.4644(8)	5.5334(16)	9.6233(22)	1.2394(4)	2.1555(6)	237.73(7)

Table 2: Refined unit-cell parameters, unit-cell volume, and axial ratios as a function of pressure from perdeuterated AMH II.

Pressure (MPa)	*a*-axis (Å)	*b*-axis (Å)	*c*-axis (Å)	*b/a*	*c/a*	Unit-cell volume (Å^3)
351.0	18.937(3)	6.970(1)	6.890(1)	0.36809(9)	0.36383(9)	909.4(2)
402.2	18.898(3)	6.958(1)	6.869(1)	0.36821(8)	0.36348(7)	903.2(3)
450.9	18.860(2)	6.948(1)	6.856(1)	0.36842(6)	0.36351(6)	898.4(2)
502.2	18.8266(5)	6.9416(2)	6.8442(2)	0.36872(1)	0.36354(1)	894.45(4)

At 180 K, the fitted 3rd order Birch-Murnaghan equation of state of AMH I has parameters, V_0 = 248.00(2) Å^3, K_0 = 7.33(3) GPa with the first pressure derivative of K_0 fixed at the value obtained in *ab initio* calculations, $(\partial K_0/\partial P)_T = K_0' = 5.3$; the implied value of the second derivative is therefore $(\partial^2 K_0/\partial P^2)_T = K_0'' = -0.94(1)$ GPa^{-1}. At 351 MPa, the transition from AMH I to AMH II occurs with an associated reduction in molar volume of 4.6 %, and an increase in the incompressibility of 19.6 %.

The equation of state results are described in more detail in Fortes *et al.* (2009b)

The AMH II crystal structure

The crystal structure of AMH II was solved using a combination of *ab initio* computational structure prediction, and structure solution from neutron powder diffraction data using direct space methods. AMH II crystallizes in space-group P*bca* with sixteen formula units in a unit-cell of dimensions *a* = 18.8285(4) Å, *b* = 6.9415(2) Å, *c* = 6.8449(2) Å, and V = 894.61(3) Å^3 [$\rho_{calc}^{deuterated}$ = 1187.56(4) kg m^{-3}] at 502 MPa, 180 K. The structure is found to be characterized by sheets of tessellated pentagons formed by orientationally ordered O—D···O, O—D···N, and N—D···O hydrogen-bonds; these sheets are stacked along the *a*-axis and connected by N—D···O hydrogen bonds alone (**Figure 2**). The hydrogen bonds along the *c*-axis water-water chains in the sheet are ordered in one particular orientation. It is possible to adopt an alternate ordered orientation, which was found by the DFT prediction, or to combine them to form a disordered crystal. The data clearly favour the first ordered orientation. The pentagonal sheets in AMH II are very similar to those found in the tetragonal argon clathrate structure (Manakov *et al*., 2004) and to those found in the semi-clathrate structures such as pinacol hexahydrate (Kim & Jeffrey, 1970). The sheets in AMH II differ from each of these by virtue of the ammonia bonded into the rings, which gives the sheets a distinct 'upper' and 'lower' surface (**Figure 2b**). As a

result, the sheets can bond directly to one another 'face to face' or 'back to back' via the second symmetry independent ammonia (**Figure 2c**).

Figure 2a shows a view of the pentagonal ribbons down the *a*-axis (with the *c*-axis vertical). The direction of the O—D···O H-bonds is shown by the red arrows (the return bonding across the pentagonal apex is indicted by small pink arrows), resulting in a net-directionality indicated by the large pink arrows. Adjacent ribbons lying in the same plane bond to one another roughly along the *b*-axis (dashed blue bonds) to form a pentagonally tessellated sheet. A view of this sheet along the *c*-axis (with the *a*-axis vertical) is shown in **Figure 3b**; note the boat conformation of individual pentagonal ribbons, and note the symbol (⊙) indicating the direction of hydrogen bonds in the crankshafts is coming out of the plane of the illustration.
The packing of these sheets is depicted in **Figure 3c**, also viewed along the *c*-axis, with the *a*-axis vertical and the *b*-axis horizontal. The glide planes generate adjacent offset sheets, with the hydrogen bonding along the crankshafts coming out of the plane of the illustration (⊙), related by the centre of symmetry to sheets with the hydrogen bonding along the crankshafts going into the plane of the illustration (⊗).

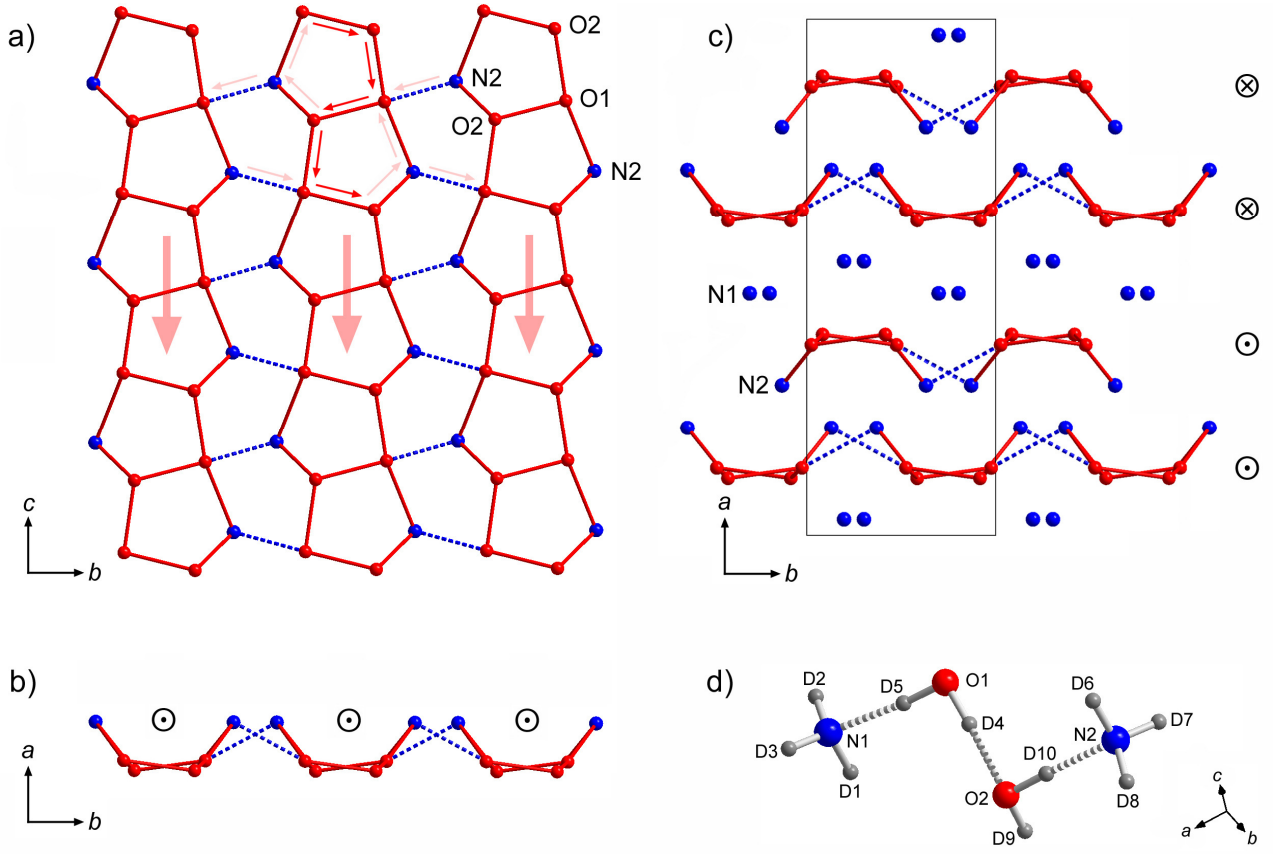

The AMH II crystal structure is described in more detail in Fortes *et al.* (2009c)

References

Fortes, A. D. *et al.* (2009a) *J. Appl. Cryst.,* **42**(5), 846-866.
Fortes, A. D. *et al.* (2009b) *J. Chem. Phys.* **131**(15), article 154504.
Fortes, A. D. *et al.* (2009c) *J. Am. Chem. Soc.,* **131**(37), 13508-13515.
Manakov, A. Yu., *et al.* (2004) *J. Incl. Phenom. Macrocycl. Chem*. **48**, 11-18.
Kim, H. S., & Jeffrey, G. A. (1970) *J. Chem. Phys.* **53**(9), 3610-3615.